Preliminary Strength Measurements of High Temperature Ash Filter Deposits

B.S.Kang (Kang@cemr.wvu.edu; (304)293-3111)
E.K.Johnson (Johnson@cemr.wvu.edu; (304)293-3111)
R. Mallela
J.F.Barberio
Mechanical and Aerospace Engineering Department
West Virginia University
Morgantown, WV 26506, U.S.A.

Introduction

The objective of this study is to develop and evaluate preliminary strength measurement techniques for high temperature candle filter ash deposits. The efficient performance of a high temperature gas filtering system is essential for many of the new thermal cycles being proposed for power plants of the future. These new cycles hold the promise of higher thermal efficiency and lower emissions of pollutants. Many of these cycles involve the combustion or gasification of coal to produce high temperature gases to eventually be used in gas turbines. These high temperature gases must be relatively free of particulates. Today, the candle filter appears to be the leading candidate for high temperature particulate removal.

The performance of a candle filter depends on the ash deposits shattering into relatively large particles during the pulse cleaning (back flushing) of the filters. These relatively large particles fall into the ash hopper and are removed from the system. Therefore, these particles must be sufficiently large so that they will not be re-entrained by the gas flow. The shattering process is dictated by the strength characteristics of the ash deposits. Consequently, the objective of this research is to develop measurements for the desired strength characteristics of the ash deposits.

The strength characteristics of an ash deposit is a function of it's environment. Experimentally, it has been found that the deposit layer next to the filter surface has been extremely difficult to remove. This inner layer is referred to as a hard deposit. The outer layer of the deposit, which is much easier to remove, is referred to as soft deposit. Obviously, the notation comes from handling the two types of deposits. The deposits employed in this study were obtained from an operating power plant. Both soft and hard deposits were readily identified. To date, the strength measurements have concentrated on the normal strain and the Young’s modulus of the deposits.

Background

The basic geometry of an ideal ash deposit on a candle filter is schematically shown in Figure 1. The ash deposit is of uniform thickness over the entire surface of the filter. A simple stress model is shown in Figure 2 for the ash deposit during the pulse cleaning, just prior to the shattering of the deposit. With the assumed symmetry, the dominant stresses are 1) the normal (hoop) stresses for the soft and hard deposits ($\sigma_{\theta\theta}^{S}$ and $\sigma_{\theta\theta}^{H}$), and the adhesive stress (σ_A) between the hard deposit and the filter surface. The pressure due to pulse cleaning is shown as P_2. The adhesive stress is due to particles becoming wedged into the pores of the filter and forming a rather hard, ridged, structure. Additional particles impacting this layer will stick to the layer and will be wedged tighter into the structure as the continuing stream particles impact the structure. The particles arriving later do not undergo the continuing impacts and subsequently do not form as rigid a structure. In addition, at the high temperatures encountered in these systems, the potential for a chemical reaction forming bonds is significant. With pulse cleaning, the reversed flow of gases only remove particles in the weaker portion of the structure.

The formation of the ash deposits depend on: 1) the particle size distribution of the dust, 2) the face velocity, 3) ash chemistry, and 4) the pressure and temperature of the gases. Ash samples from an operating power plant were obtained from DOE/METC for this study so that these measurements might proceed in an expeditious manner.

Experimental Approach and Results

Room Temperature Tests

The approach developed in this research to measure the strength characteristics of ash deposits at room temperature is to glue a filter cake (ash deposit) specimen to a flexural beam. An aluminum beam was used in the room temperature tests. A load is then applied to the beam to produce a known bending moment in the beam as shown in Figure 3. The attached specimens were obtained by cutting the as-received large "chunks" of ash deposits into flat slabs to fit onto the beam. This procedure was rather tedious due to the softness of the ash deposits and relatively large particles in the ash sample which made it difficult to obtain a smooth surface. The cutting process was continued until smooth parallel surfaces were obtained on the specimen. The specimen was then glued to the beam using epoxy. The experiment consisted of loading the beam incrementally and recording the strain gage readings. A long distance microscope fitted with a color CCD camera and monitor was used to inspect the surface of the specimen for crack initiation site and an analog video printer was used to print out the images, as shown in Figure 3. The loading was continued until the formation of an initial crack was detected.

The analysis of the data for the room temperature tests were based on the model shown in Figure 4. As shown, the strain distribution was assumed to vary linearly in the beam and the cake specimen. The unknowns to be determined are the maximum cake strain $(\varepsilon_{cake})_{max}$ and modulus of elasticity (E_1) of the filter cake. The dimensions, a and b, and the modulus of elasticity of the aluminum beam (E_2) are known. The strain (ε_0) along the underside of the beam can be determined based on linear interpolation of the two strain gage readings. The equations for calculating the unknowns are

$$(\epsilon_{cake})_{\max} = \frac{\epsilon_0(c+a)}{(c-b)}$$

$$E_1 = \frac{-B+\sqrt{(B^2-4a^4C)}}{2a^4}$$

Where

$$B = 2ab(3ab+2a^2+2b^2)E_2+6a(a+2b)\frac{M}{\epsilon_o}$$

$$C = b^2E_2(\frac{6M}{\epsilon_0}+b^2E_2).$$

A total of four tests (two hard deposits and two soft deposits) were conducted. Figures 5 to 8 show the test results also shown in the figures are the dimensions of the ash samples. Figures 9 to 12 show load versus ash deposit strain plots. Tables 1 to 4 show the tabulated results for each test. Finally, Table 5 shows the summary results. These results show quite consistent failure tensile strain values for the hard deposit as well as the soft deposit. However, Test No. 2 of the hard deposit showed substantially higher Young's modulus value comparing to Test No.1. This may due to the fact that SuperGlue was used in Test No. 2 to bond the ash cake to the beam. The SuperGlue may have penetrated into the ash deposit creating an artificial stiffness of the filter cake. For the rest of the room temperature tests, a high viscosity epoxy was used and no glue penetration was observed.

Elevated Temperature Test Results

Two types of elevated temperature tests were conducted. The first type of test consisted of using a bending beam (BB) apparatus, as shown in Figures 13 and 14. The second type of test involved employing a thermal expansion mismatch (TEM) measurement procedure to obtain the failure tensile strain of ash deposit. Both the beam and the bending apparatus are made of IN718 superalloy. All the elevated temperature tests were conducted on soft ash deposits. The BB tests were performed at 1200^0F and the TEM tests were performed at a much lower elevated temperature.

The BB tests consisted of placing a thin (0.06 inch) specimen on the IN718 beam, and the whole bending beam apparatus was then put inside a furnace. The furnace was heated to 1200^0F. At this temperature, the furnace was opened and both ends of the specimen were glued to the beam. Alumina cement was used as the glue. This approach avoided introducing the effect of thermal expansion mismatch during heating up the furnace. The beam was now loaded incrementally until a crack in the specimen was observed through the long distance microscope. Figure 15 shows the results of one high temperature test. The tensile strain was calculated for the surface of the beam at each contact (glue) point using the simple bending beam formula. The

tensile strain in the specimen was then calculated as the average of the two beam surface strains. Two tests were conducted and both showed that the failure cake strain at 1200 ^{o}F is approximately 450 μ. In order to verify this approach, this test procedure was repeated at room temperature. The failure tensile strain was determined to be 1200μ, which is in good agreement with the data in Table 5.

The TEM method consisted of attaching a thin specimen to a beam. Both end of the specimen were glued to the beam using alumina cement. The test system was then placed in a furnace and the temperature was slowly increased until a crack in the specimen was observed. The initiation of a crack was again detected using a long distance microscope. Four tests were performed, each showed a crack appeared at a temperature of 190^{0}F. A typical test result is shown in Figure 16. From the equation

$$\varepsilon_{cake} = (\alpha_{718} - \alpha_{cake})\,\Delta T = (7.2*10^{-6} - 4.0*10^{-6})*(190°F - 80°F) = 352\ \mu$$

The failure tensile strain of the ash deposit at 190^{0}F is then determined.

Figure 17 shows the failure tensile strain as a function of temperature for a soft ash deposit. The rapid decrease of the failure tensile strain with temperature is probably due to the removal of moisture in the ash deposit specimen.

Conclusion

Experimental procedures were developed to measure Young's modulus of the ash deposit at room temperature and the failure tensile strain of ash deposits from room temperature to elevated temperatures. Preliminary data has been obtained for both soft and hard ash deposits. The qualifier "preliminary" is used to indicate that these measurements are a first for this material, and consequently, the measurement techniques are not perfected. In addition, the ash deposits tested are not necessarily uniform and further tests are needed in order to obtain meaningful average data.

Acknowledgment

This research was jointly supported by METC and WVU NRCCE. We would like to express our appreciation to R. Dennis and T.K.Chiang at METC for their support and encouragement of this exploratory research effort.

Table 1 Experiment No. 1 Hard Deposit

Load (N)	ϵ_0 (10^{-6} m/m)	$(\epsilon_{cake})_{max}$ (10^{-6} m/m)	Young's Modulus (GPa)
9.86	-192.64	401.11	8.93
19.72	-385.84	803.39	8.76
41.95	-827.52	1723.05	8.54
63.93	-1209.80	2519.03	9.70
81.77 *	-1585.00	3300.27	9.01

* Crack initiation.

Table 2 Experiment No. 2 Hard Deposit

Load (N)	ϵ_0 (10^{-6} m/m)	$(\epsilon_{cake})_{max}$ (10^{-6} m/m)	Young's Modulus (GPa)
22.36	-405.60	764.40	35.62
41.10	-779.70	1469.43	30.36
59.83	-1161.70	2189.35	28.03
80.36	-1571.00	2960.70	27.34
91.56 *	-1834.90	3458.08	25.03

* Crack initiation.

Table 3 Experiment No. 1 Soft Deposit

Load (N)	ϵ_0 (10^{-6} m/m)	$(\epsilon_{cake})_{max}$ (10^{-6} m/m)	Young's Modulus (GPa)
2.24	-51.20	173.18	0.27
4.48	-102.10	345.35	0.31
8.96	-204.10	690.36	0.32
13.44	-306.40	1036.39	0.31
17.92 *	-401.10	1380.39	0.32

* Crack initiation.

Table 4 Experiment No. 2 Soft deposit

Load (N)	ϵ_0 (10^{-6} m/m)	$(\epsilon_{cake})_{max}$ (10^{-6} m/m)	Young's Modulus (GPa)
2.24	-98.50	301.97	0.35
4.48	-197.20	604.55	0.33
6.72	-291.60	893.95	0.31
8.96 *	-393.80	1207.26	0.36

* Crack initiation.

Table 5 Room Temperature Tests

Test	Filter Cake	Thickness (10^{-3} m)	Temperature	Filter Cake Tensile Strain (10^{-6} m/m)	Young's Modulus (GPa)
1	Hard	5.08	Room	3300.27	8.988
2	Hard	3.048	Room	3456.38	29.276
3	Soft	3.81	Room	1380.39	0.306
4	Soft	3.302	Room	1207.26	0.3375

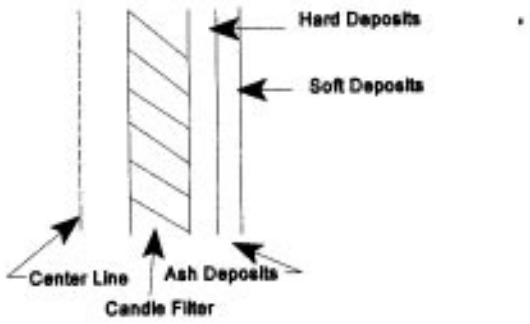

Figure 1 Schematic drawing of ideal ash deposit on a candle filter.

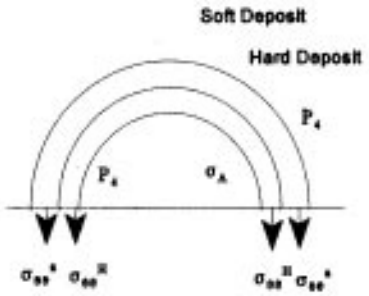

Figure 2 Stress model for ash deposit during pulse cleaning.

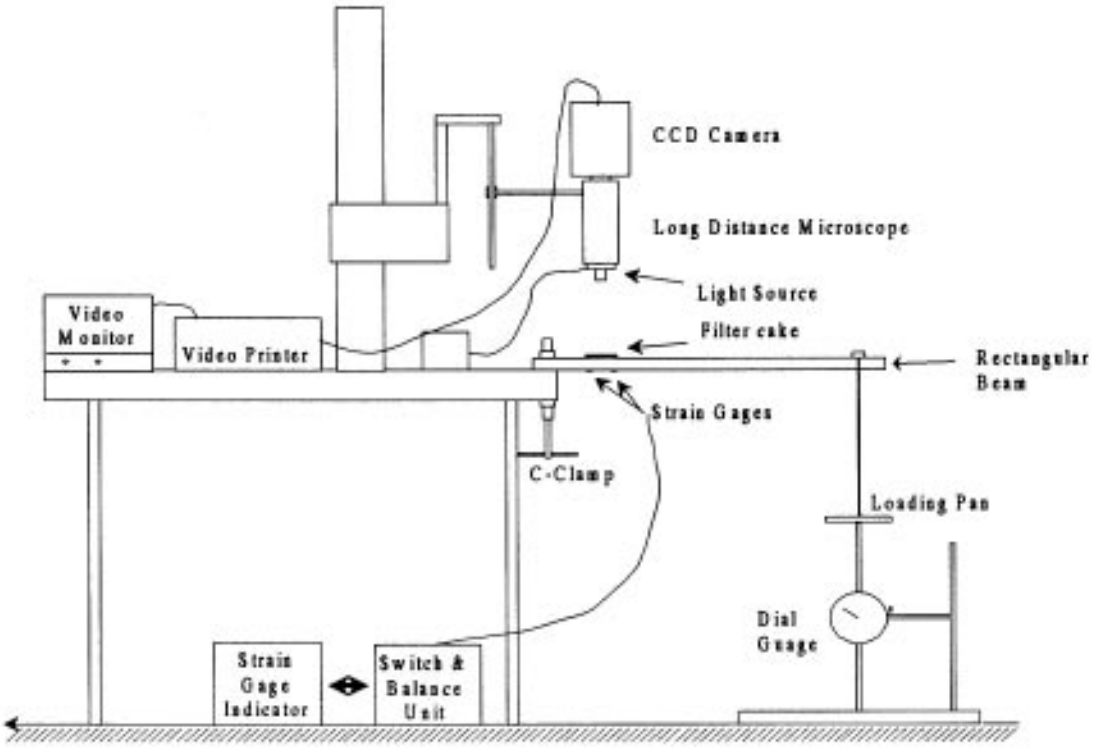

Figure 3 Room temperature filter cake strength test setup.

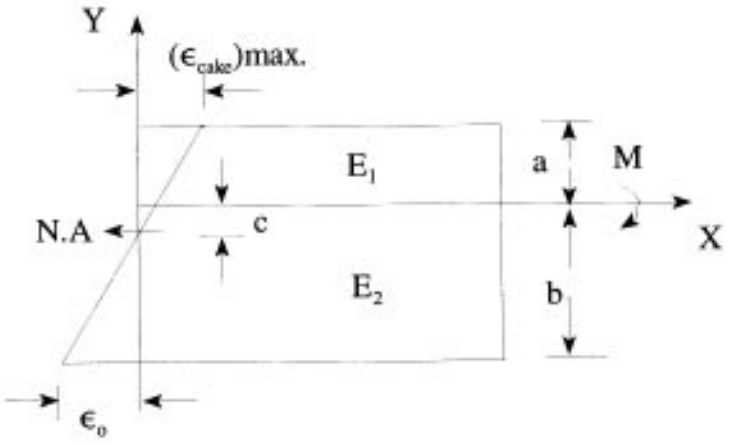

E_1 = Young's modulus of the ash deposit

E_2 = Young's modulus of the beam material

M = Applied bending moment

ϵ_0 = Strain gage reading

N.A = Neutral axis

a = Ash deposit thicknes

b = Beam thicknes

Figure 4 Analytical model for filter cake strain and Young's modulus determination.

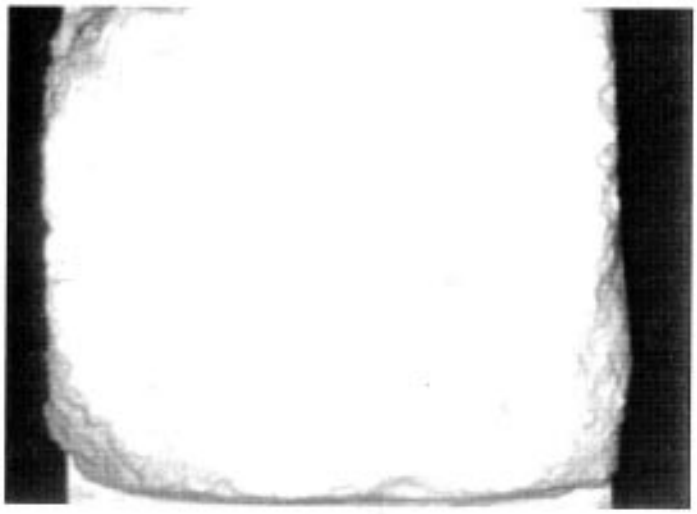

BEFORE LOADING

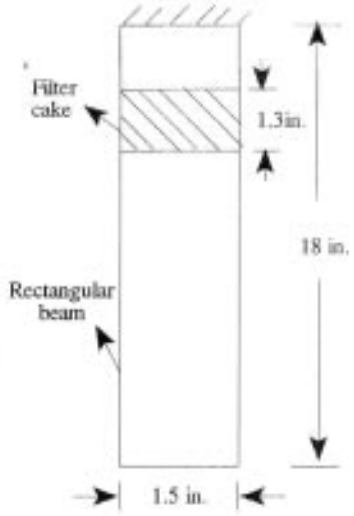

CRACK INITIATION

Figure 5 Hard ash deposit test no. 1.

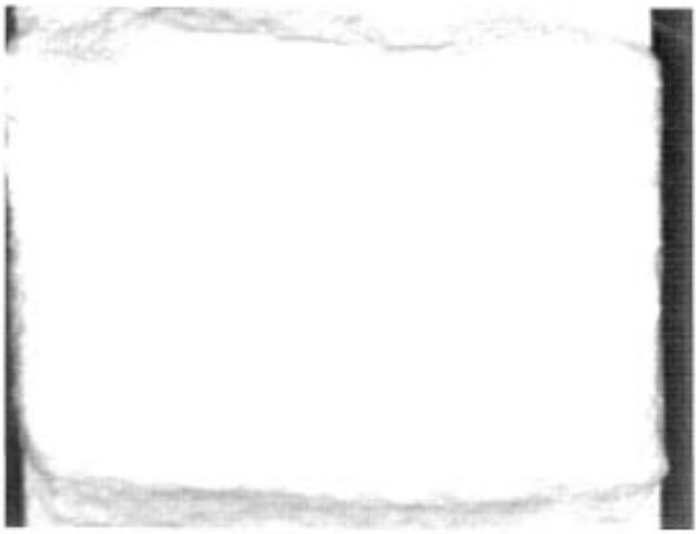

BEFORE LOADING

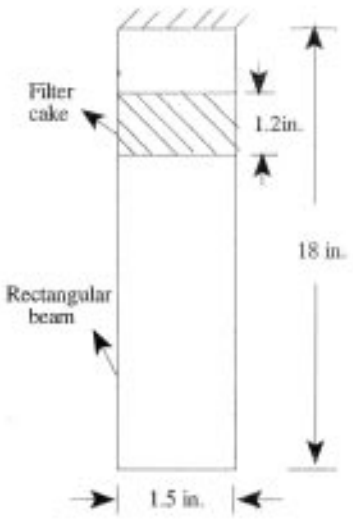

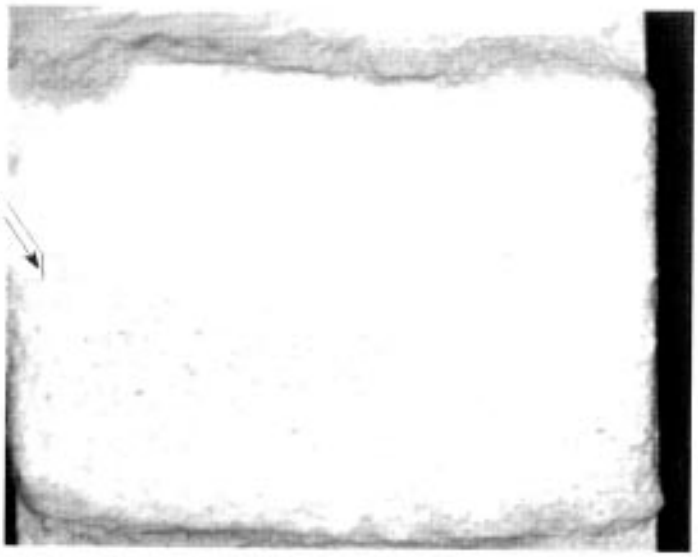

CRACK INITIATION

Figure 6 Hard ash deposit test no. 2.

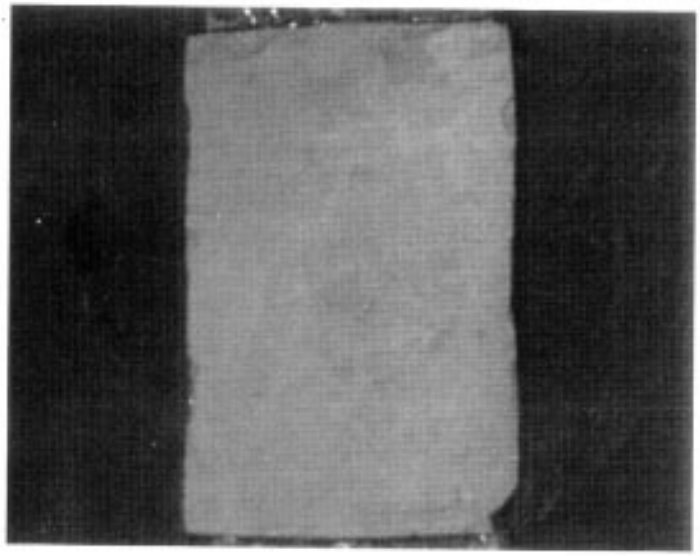

BEFORE LOADING

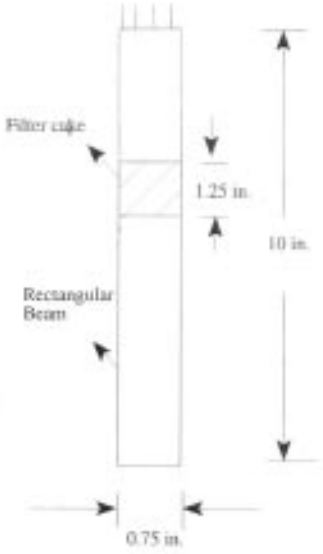

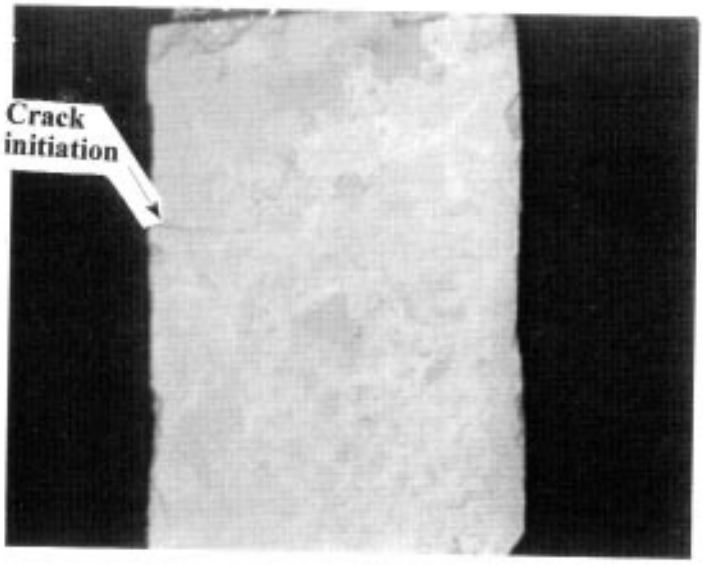

CRACK INITIATION

Figure 7 Soft ash deposit test no. 1.

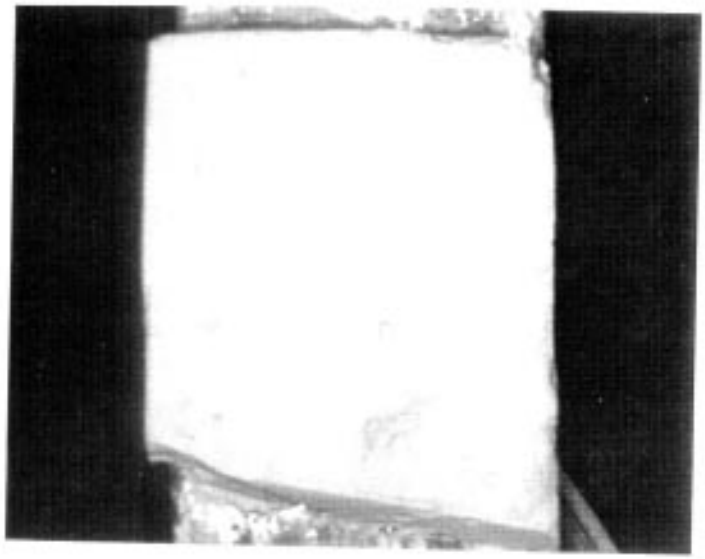

BEFORE LOADING

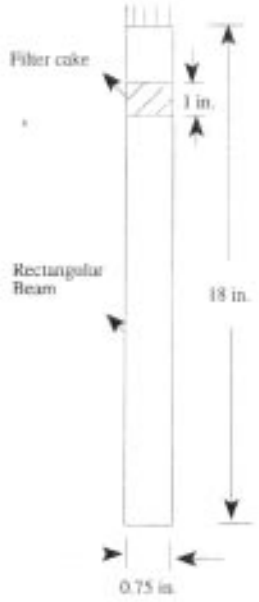

CRACK INITIATION

Figure 8 Soft ash deposit test no. 2.

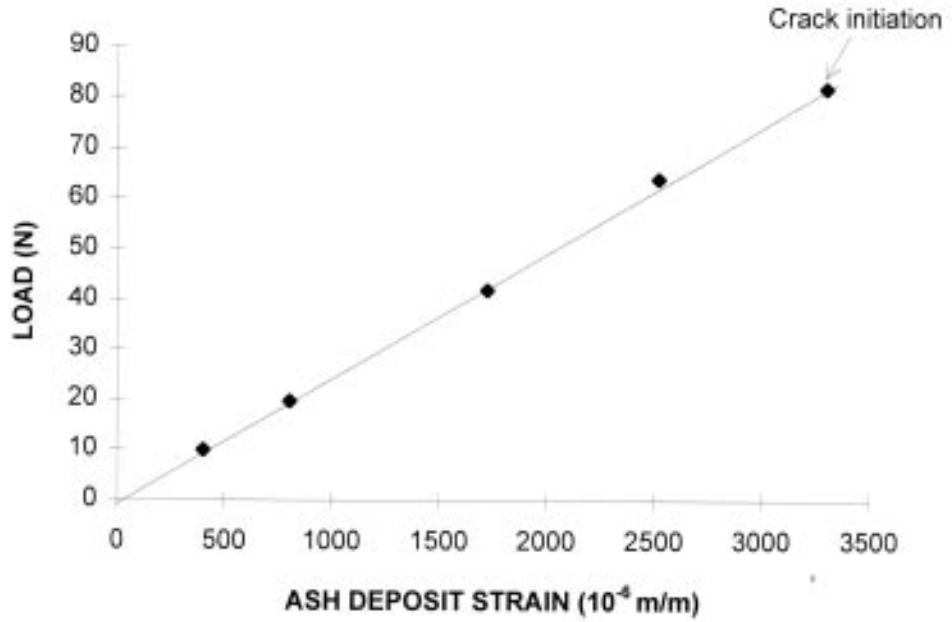

Figure 9 Load versus ash deposit strain plot.
(Hard ash deposit, test no. 1)

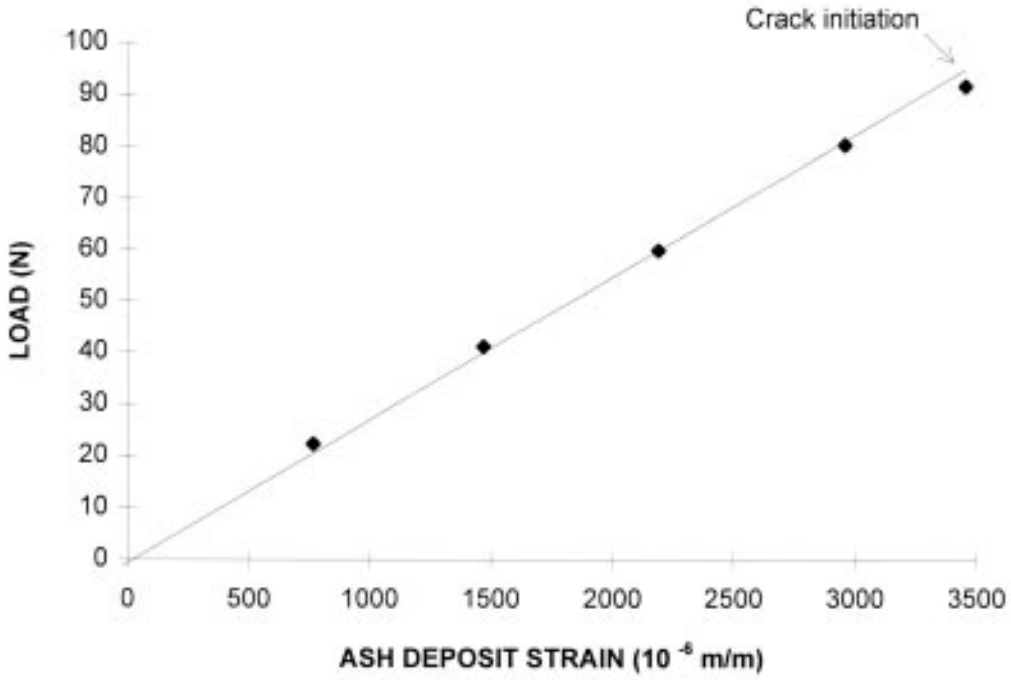

Figure 10 Load versus ash deposit strain plot.
(Hard ash deposit, test no. 2)

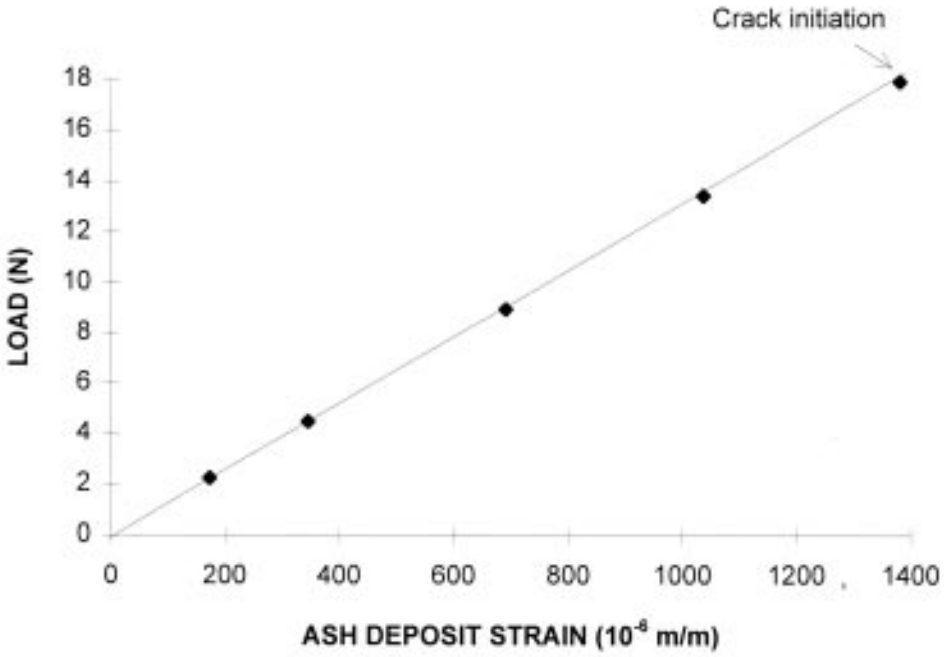

Figure 11 Load versus ash deposit strain plot.
(Soft ash deposit, test no. 1)

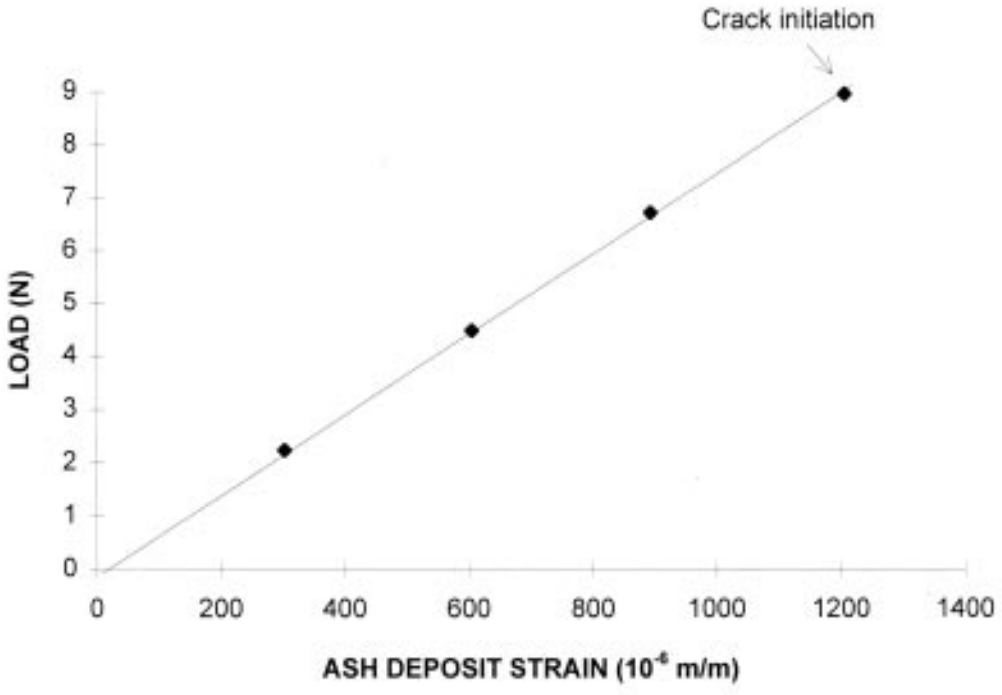

Figure 12 Load versus ash deposit strain plot.
(Soft ash deposit, test no. 2)

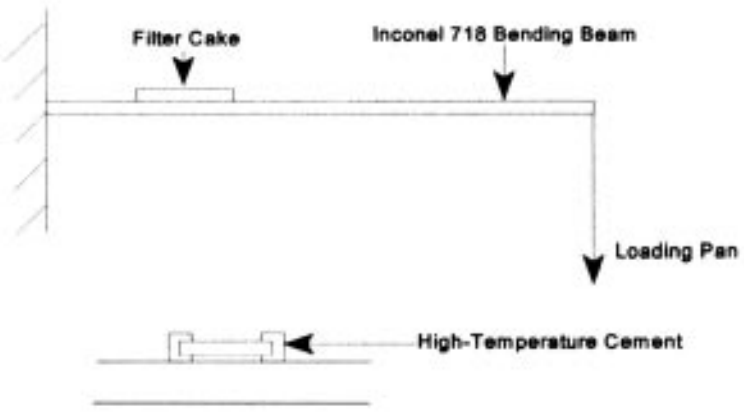

Figure 13 Schematic drawing of ash specimen layout for high temperature test or thermal expansion mismatch measurement.

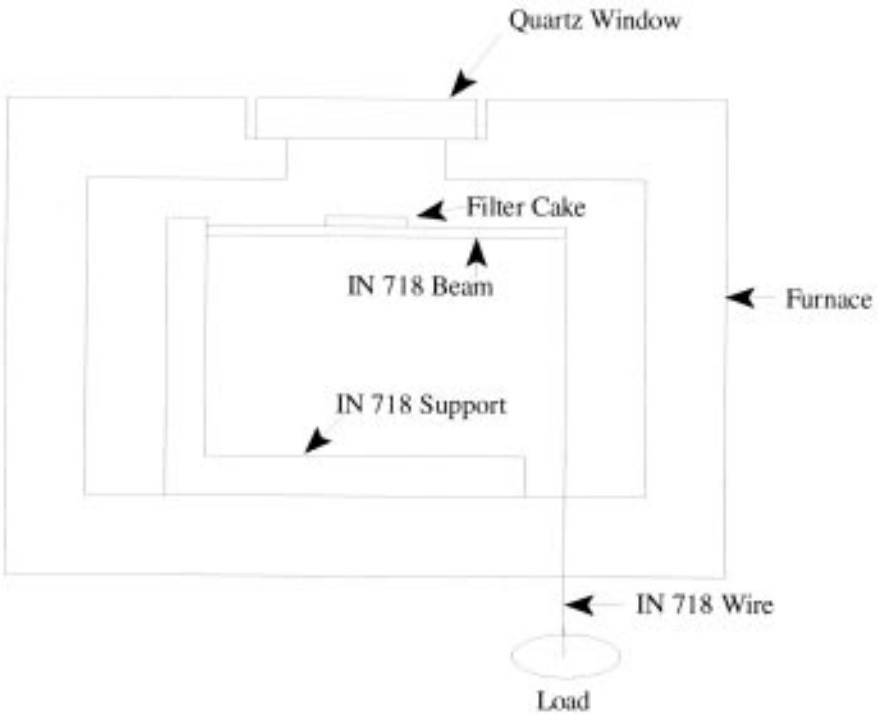

Figure 14 Schematic drawing of high temperature ash strain measurement test setup.

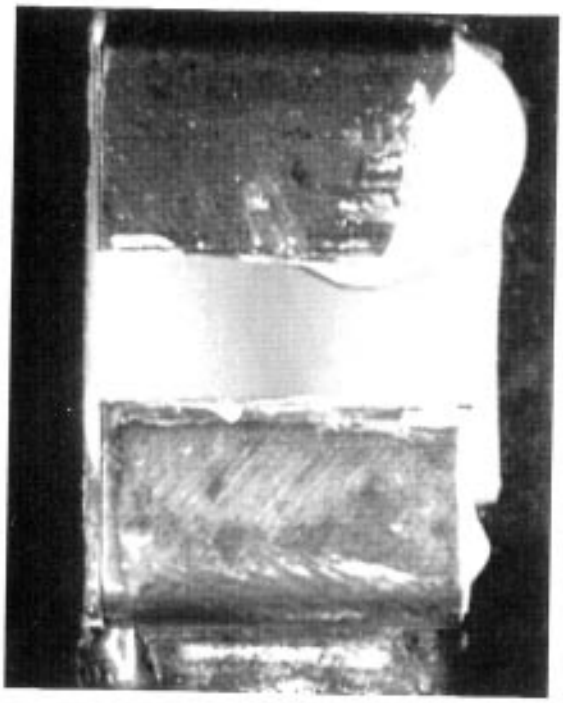

T = 80 °F
(NO LOAD)

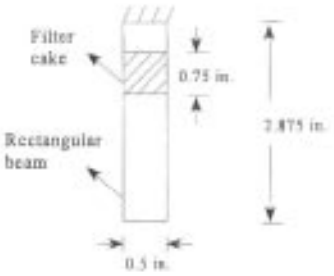

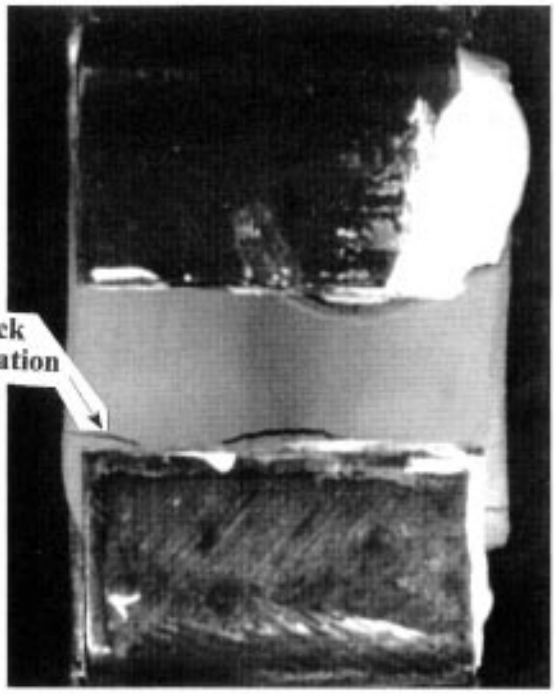

T = 1200 °F
(WITH APPLIED LOAD)

Figure 15 Typical high temperature test result.

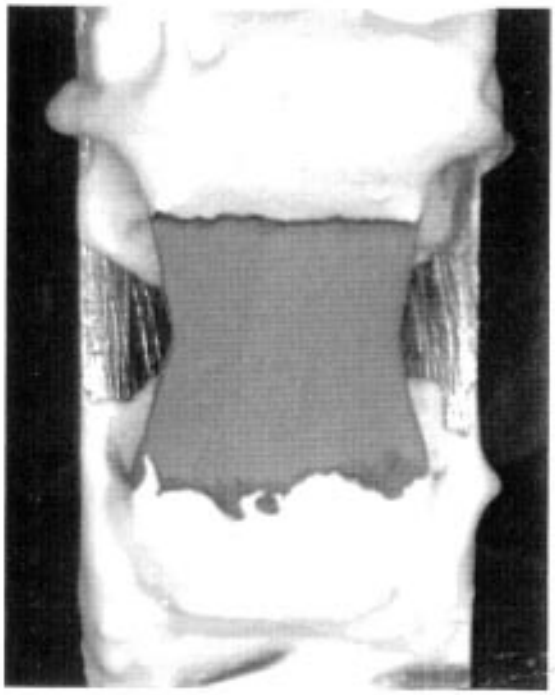

, T = 80 °F

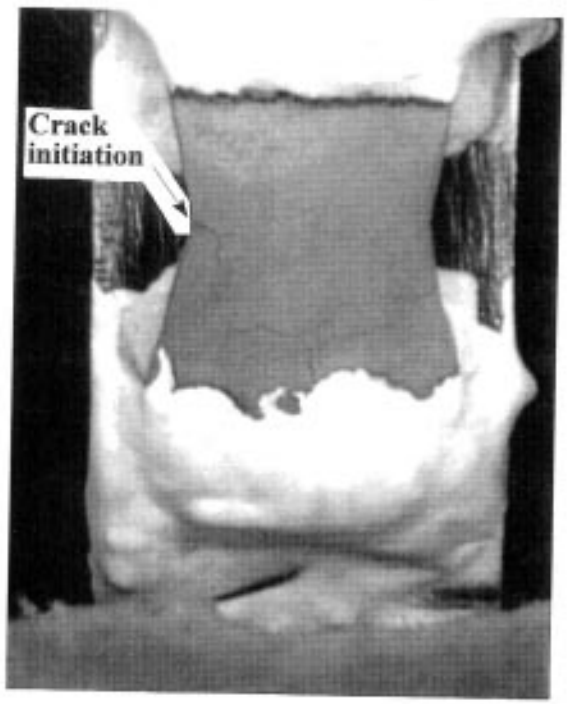

T = 190 °F

Figure 16 Typical thermal expansion mismatch test result.

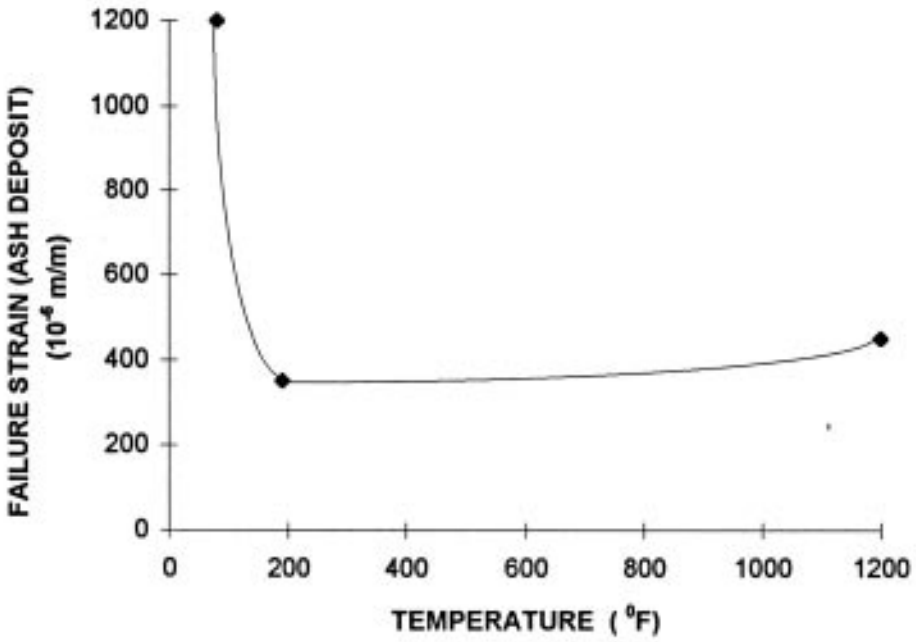

Figure 17 Ash deposit strain versus temperature plot.